Materials Horizons

COMMUNICATION

View Article Online
View Journal | View Issue

Check for updates

Cite this: *Mater. Horiz.*, 2018, 5, 868

Received 2nd May 2018,
Accepted 21st June 2018

DOI: 10.1039/c8mh00511g

rsc.li/materials-horizons

Published on 21 June 2018. Downloaded by Brown University on 4/15/2019 6:26:14 PM.

Integration of a functionalized graphene nano-network into a planar perovskite absorber for high-efficiency large-area solar cells†

Yong Wang,[a] Yuanyuan Zhou,[b] Taiyang Zhang,[a] Ming-Gang Ju,[c] Lin Zhang,[b] Miao Kan,[a] Yihui Li,[a] Xiao Cheng Zeng,[c] Nitin. P. Padture[b] and Yixin Zhao*[a]

Efficient charge collection is critical in large area (quasi-) planar configuration perovskite solar cells (PSCs) as the cell operation relies on the diffusion of photo-generated charge carriers to charge collector layers. Many defects/traps in the polycrystalline perovskite absorber layer strongly affect the charge collection efficiency because the 2D-like top charge collection layer barely penetrates into the 3D grain boundaries in the perovskite layer to efficiently collect the charge carrier. Inspired by blood capillaries for efficient mass exchange, a charge-collection nano-network for efficient charge collection was incorporated into the perovskite absorber using low-cost, stable amino-functionalized graphene (G-NH_2). The integration of such an unprecedented structure enables very efficient charge collection, leading to the significant enhancement of the power conversion efficiency of 1 × 1 cm^2 $MAPbI_3$ PSCs from 14.4 to 18.7% with higher reproducibility, smaller hysteresis and enhanced stability. The physicochemical mechanisms underlying the role of this nano charge-collection nano-network in boosting the charge collection in PSCs are elucidated comprehensively, using a combined experimental and theoretical approach, pointing to a new direction towards up-scaling of high-efficiency PSCs.

Conceptual insights

High charge collection efficiency in lead halide perovskite solar cells is most critical to their high efficiency for commercialization of this promising low-cost and high-efficiency photovoltaic technology. In (quasi)-planar configuration perovskite solar cells, charge collection occurs at the 2D interface between a perovskite absorber top surface layer and a planar charge collection layer. The large number of grain boundaries, likely distributed three dimensionally, in this polycrystalline perovskite absorber layer could hinder the charge collection efficiency. In this study, we demonstrated a quasi-3D charge collection nano-network configuration for the design of large-area planar perovskite solar cells with enhanced collection efficiency. The integration of an unprecedented functionalized graphene nano-network into the perovskite absorber layer leads to the formation of a quasi 3D charge collection layer combined with a typical 2D charge-collection layer. This quasi 3D charge collection configuration significantly enhances the power conversion efficiency of 1 × 1 cm^2 $MAPbI_3$ PSCs from 14.4 to 18.7% with higher reproducibility, smaller hysteresis and enhanced stability. The concept of introducing a quasi-3D charge collection configuration into a perovskite absorber layer would be a promising strategy to pave the way for high-performance and large area perovskite solar cell devices.

Introduction

Perovskite solar cells (PSCs), with unprecedented progress in their power conversion efficiency (PCE), have enormous potential as next-generation photovoltaics (PVs) for the clean-energy future.[1–3] The certified record PCE of PSCs has quickly approached 23%, which is comparable to the PCEs of crystalline silicon solar cells.[4] In general, PSCs employ solution-deposited polycrystalline organic–inorganic halide perovskite thin films as the light absorber.[5,6] Due to the high-density of grain boundaries (GBs), these polycrystalline perovskite thin films contain abundant defects/traps to deteriorate the charge collection efficiency.[7,8] Reducing defects/traps in the perovskite absorber layer, and thereby improving the charge-collection efficiency in PSCs, has become one of the most popular strategies for achieving maximum PCE, which is critical for the successful commercialization of this promising low-cost, high-efficiency PV technology.[9]

The state-of-the-art high-efficiency PSCs are invariably based on (quasi-) planar device configurations, where two charge collection layers (CCLs) sandwich a perovskite absorber layer to collect the charge carriers that are generated in the perovskite bulk and diffuse to the perovskite/CCL interfaces.[10–13] The charge collection process occurs mainly at the interface between the perovskite absorber layer and the CCLs. The carrier diffusion lengths in planar perovskite thin films are considered to be long, resulting in a high charge-collection efficiency in PSCs.[14,15] Nevertheless, there is still considerable charge-collection loss due to the defects/traps at GBs in the perovskite absorber layer.[16–18]

[a] School of Environmental Science and Engineering, Shanghai Jiao Tong University, 800 Dongchuan Road, Shanghai 200240, China. E-mail: yixin.zhao@sjtu.edu.cn
[b] School of Engineering, Brown University, Providence, Rhode Island 02912, USA
[c] Department of Chemistry, University of Nebraska-Lincoln, Lincoln, Nebraska 68588, USA

† Electronic supplementary information (ESI) available. See DOI: 10.1039/c8mh00511g

This journal is © The Royal Society of Chemistry 2018

Published on 21 June 2018. Downloaded by Brown University on 4/15/2019 6:26:14 PM.

Such charge-collection loss can be even more severe in large-area PSC devices, which not only reduces their PCEs but also lowers the device reproducibility.[19,20] One straightforward strategy to increase the charge-collection efficiency is to enhance or modify the charge-collection interfaces.[21,22] In the literature, carbon-based materials with excellent charge transfer properties and high chemical stability have been employed as a new charge collection layer or as a modifier in the existing charge-collection layer in PSCs.[23–25]

Inspired by the effective mass exchange in blood capillaries, we demonstrate an unprecedented strategy to boost the charge collection in PSC devices *via* incorporating a carbon-based charge-collection nano-network into the $CH_3NH_3PbI_3$ ($MAPbI_3$) perovskite absorber layer. The construction of the carbon-based charge collection nano-network was realized *via* simply adding amino-functionalized graphene (G-NH_2) into the $MAPbI_3$ precursor solution, followed by co-precipitation of G-NH_2 and $MAPbI_3$ perovskite. The integration of the functionalized graphene in the perovskite layer not only induces the formation of large grain size perovskite crystals but also helps the formation of the nano-network in the $MAPbI_3$ perovskite absorber layer. Consequently, the 1×1 cm^2 large area $MAPbI_3$ PSCs with the *in situ* integrated nano-network exhibits power conversion efficiencies of up to 18.7% with higher reproducibility, smaller hysteresis and enhanced stability than the 14.2% efficiency control ones.

Results and discussion

Fig. 1a shows the topographic images of the as-prepared G-NH_2 taken using an atomic force microscope (AFM). The thickness of G-NH_2 is about 0.8 nm (Fig. S1, ESI†), and they possess submicron lateral size. The Fourier transform infrared spectroscopy (FTIR) spectrum in Fig. 1b confirms the amino group in these G-NH_2 samples. Also, TEM results indicate that the as-prepared G-NH_2 is composed of few-layer transparent graphene sheets with homogeneous elemental distribution of C, N on the graphene sheets (Fig. S2, ESI†). G-NH_2 can be well-dispersed in the $MAPbI_3$ precursor solution in a mixed DMF/DMSO (v/v ratio, 4 : 1) solvent. As shown in Fig. S3 (ESI†), after the addition of G-NH_2, the $MAPbI_3$ precursor solution appears darker. It is found that the introduction of G-NH_2 has some obvious effects on the microstructures of the as-deposited $MAPbI_3$ perovskite thin films. Fig. S3 (ESI†) reveals that the incorporation of G-NH_2 has a negligible effect on the UV-vis spectra of the $MAPbI_3$ perovskite films. The absorbance edges of both thin films are located at ~780 nm, which is consistent with previous results.[26] Fig. 1c and d show that both $MAPbI_3$ and $MAPbI_3$/G-NH_2 thin films are compact, pinhole-free, and with full-coverage, which is typical of thin films prepared using the solvent-engineering method.[5,6,27] However, the $MAPbI_3$/G-NH_2 thin film has larger grains and smoother surface in comparison with the pure $MAPbI_3$ thin film. In the $MAPbI_3$/G-NH_2 thin film, the average grain size is >500 nm with the largest grains >1 μm, whereas the pure $MAPbI_3$ thin film has an average grain size of ~300 nm. The enlarged grains might be attributed to the high dispersion of G-NH_2 at the $MAPbI_3$ grain boundary which tailors the grain boundary migration process during the thermal annealing stage.[28] More detailed studies will be performed in the future to elucidate this effect. The 3D AFM images in Fig. S4 (ESI†) show that the root mean square (RMS) roughness of the $MAPbI_3$/G-NH_2 thin film top-surface is 6.6 nm, smaller than the 10.2 nm RMS roughness of the pure $MAPbI_3$ thin film.

The XRD patterns of both the $MAPbI_3$/G-NH_2 and pure $MAPbI_3$ perovskite thin films show strong diffraction peaks at 14.1°, 28.4° and 31.8° (Fig. 1e), which are respectively assigned to the 110, 220 and 310 reflections in the typical tetragonal phase of $MAPbI_3$ perovskite.[29] The intensity of XRD peaks for the $MAPbI_3$/G-NH_2 thin film is stronger than that for the pure $MAPbI_3$ perovskite, suggesting that the G-NH_2 incorporation enhances the overall crystallinity of the thin film. In addition, we have found that the amount of G-NH_2 incorporated into the

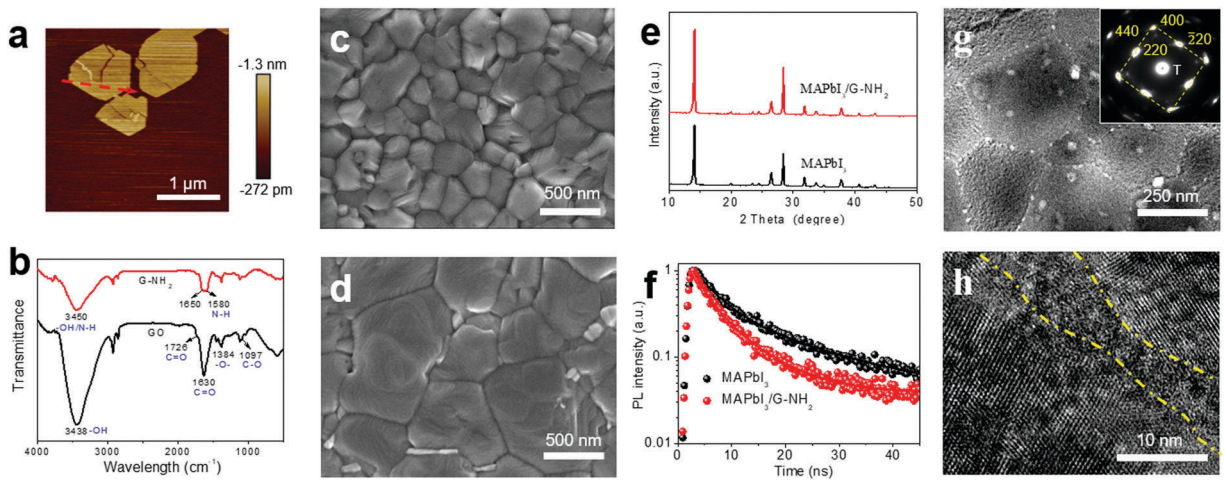

Fig. 1 G-NH_2: (a) topographic AFM image, (b) FTIR spectra of G-NH_2. SEM of thin films: (c) $MAPbI_3$ and (d) $MAPbI_3$/G-NH_2. (e) XRD patterns of the $MAPbI_3$ thin films with and without optimal G-NH_2 addition. (f) TRPL decay curves of $MAPbI_3$ and $MAPbI_3$/G-NH_2 thin films. The measurements were performed from the perovskite film side. (g) Bright-field TEM image of the $MAPbI_3$/G-NH_2 thin film, and (h) HRTEM image of the GB region (between dashed yellow lines).

Published on 21 June 2018. Downloaded by Brown University on 4/15/2019 6:26:14 PM.

$MAPbI_3$ thin films has only slight effects on the UV-vis absorption spectra, XRD patterns and grain size (Fig. S5 and S6, ESI†). These results indicate that the incorporation of G-NH_2 improves the crystallinity, enlarges the grain size, and smoothens the surface of the perovskite absorber film. This can be attributed to the relatively controlled nucleation and growth behavior induced by G-NH_2 as heterogeneous nucleation sites in the crystallization process.

Normally, enhanced crystallinity and larger grain size are expected to reduce defects/traps and then increase the photoluminescence (PL) lifetimes in perovskite thin films.[30] However, the time-resolved PL (TRPL) responses from $MAPbI_3$ and $MAPbI_3$/G-NH_2 thin films in Fig. 1f reveal that $MAPbI_3$ thin film's lifetime (τ_{av} = 10.99 ns) is almost twice longer than that of $MAPbI_3$/G-NH_2 (τ_{av} = 5.05 ns). Such abnormal decrease of PL lifetime is actually similar to the case of perovskite films covered with charge transport (carrier-quencher) layers.[31–33] The TRPL results combined with the material-characterization results in Fig. 1 indicate efficient charge extraction and interface contact between G-NH_2 and $MAPbI_3$ perovskite crystals. Furthermore, we have also investigated the effect of reduced graphene oxide (rGO) on the $MAPbI_3$ perovskite film for comparison (Fig. S7, ESI†). Similar to G-NH_2, rGO incorporation shows a similar effect of enhanced crystallinity and enlarged grain size. However, the τ_{av} = 69.23 ns for $MAPbI_3$/rGO thin film is much longer than that for pure $MAPbI_3$ (Fig. S7, ESI†), suggesting the poor charge extraction by rGO.

In order to confirm the detailed microstructure, transmission-electron-microscopy (TEM) characterization of the $MAPbI_3$/G-NH_2 thin film was performed. The TEM specimens were prepared using a methodology that has been successfully demonstrated for characterizing halide perovskite materials in previous reports.[29,34] This entails direct solution-deposition of the $MAPbI_3$/G-NH_2 thin film onto the TEM grid. Fig. 1g is a bright-field TEM image of the $MAPbI_3$/G-NH_2 thin film. The perovskite grains and GBs areas are immediately differentiated from the contrast, and are labelled in Fig. 1g. The typical selected-area electron diffraction pattern (SAEDP) of an individual grain is shown in the inset image in Fig. 1g, which confirms the single-crystalline nature of the grains. The indexed SAEDP is consistent with the tetragonal phase of $MAPbI_3$ perovskite.[29] High-resolution TEM images of the typical GB regions were also obtained, and the result is shown in Fig. 1h. It can be seen that the GB region appears relatively amorphous, which is clearly distinct from the high-crystalline state of the $MAPbI_3$ perovskite grain. It appears that the GB regions are decorated with the carbonaceous material (G-NH_2), which is consistent with the AFM results.

These results taken together indicate that the G-NH_2 layer buried in the perovskite absorber layer forms a G-NH_2 nano-network, which has the potential to facilitate charge extraction and transport in planar PSCs. Here is another important thing that we have to note: the PSC devices integrated with the G-NH_2 nano-network show much less shorting than the control ones. This fact also suggests that the G-NH_2 layer is highly likely to be buried in the perovskite absorber layer. Further, a typical planar device configuration of FTO/c-TiO_2/SnO_2/perovskite/Spiro-OMeTAD/Ag (Fig. S8, ESI†) is adopted for both $MAPbI_3$/G-NH_2- and $MAPbI_3$-based PSCs. $MAPbI_3$/G-NH_2 based devices with an area of 0.1 cm^2 and different G-NH_2 contents have been investigated firstly (Fig. S9 and S10, ESI†), and the optimized G-NH_2 content is found to be 0.05 mg mL^{-1} (hereafter, $MAPbI_3$/G-NH_2 refers to thin films with optimized 0.05G-NH_2 content.). The PV performance statistics in Fig. S10 (ESI†) show that all $MAPbI_3$/G-NH_2-based PSCs exhibit higher PV performance than PSCs based on pure $MAPbI_3$. Moreover, the $MAPbI_3$/G-NH_2-based PSCs show an important advantage of both enhanced reproducibility with a narrow PCE distribution and small hysteresis in *J–V* curves (Fig. S11, ESI†). The champion of $MAPbI_3$/G-NH_2-based PSC exhibits enhanced PV performance over the $MAPbI_3$ one (20.4% *vs.* 18.5%) (Table S1, ESI†).

The application of large area PSC devices has been impeded by the significant reduction of PCEs and the poor device reproducibility once the cell area increases. One main reason is that the large area PSC devices are sensitive to defects/traps and charge transfer properties.[19,20,35] Interestingly, the incorporation of a G-NH_2 nano-network into the perovskite absorber layer could significantly improve both the PCE and reproducibility of large-area devices. The PV performance parameter statistics in Fig. 2a and Table S2 (ESI†) are obtained from 2.5 × 2.5 cm^2 substrates with an effective cell area of 1 cm^2, and the $MAPbI_3$/G-NH_2 based PSCs are based on the optimum G-NH_2 content as the aforementioned small area ones. Excitingly, the large-area $MAPbI_3$/G-NH_2-based PSCs exhibit an average efficiency as high as 17.4%, while the $MAPbI_3$-based PSCs only have a value of 13.2%. The efficiency distribution of $MAPbI_3$/G-NH_2-based PSCs is narrower than the pure $MAPbI_3$ based PSCs, suggesting an enhanced reproducibility. Fig. 2b compares the *J–V* curves of the champion large-area $MAPbI_3$/G-NH_2 and $MAPbI_3$ based PSCs. The $MAPbI_3$/G-NH_2-based device shows a PCE of 18.7% with a J_{SC} of 22.8 mA cm^{-2}, V_{OC} of 1.11 V and FF of 0.739. In contrast, the champion large-area cell with the $MAPbI_3$ thin film without the G-NH_2 has a PCE of only 14.4% due to the lower J_{SC} of 21.1 mA cm^{-2}, lower V_{OC} of 1.08 V, and a significantly lower FF of 0.632. The large-area $MAPbI_3$/G-NH_2-based PSCs also exhibit smaller hysteresis (Fig. S12 and Table S3, ESI†), and finally result in a stable 18.0% PCE output (Fig. S13, ESI†). The external quantum efficiency (EQE) of the $MAPbI_3$/G-NH_2-based PSC in Fig. 2c can be as high as 92% in the wavelength range of 500–600 nm, which is much higher than that of the corresponding pure $MAPbI_3$. Since there is no difference in the absorbance between $MAPbI_3$ and $MAPbI_3$/G-NH_2 thin films (Fig. S3, ESI†), the enhanced J_{SC} is attributed to the improved charge-collection efficiency in $MAPbI_3$/G-NH_2 with the help of the charge collection nano-network. The integrated J_{SC} calculated from the EQE is 22.6 mA cm^{-2}, whereas the pure $MAPbI_3$ device shows an integrated J_{SC} value of 21.0 mA cm^{-2} (Fig. 2c). These EQE results are consistent with the *J–V* measurements, and confirm the enhanced charge-collection efficiency in the $MAPbI_3$/G-NH_2-based PSC. Moreover, the lower electronic resistance (~13 Ω) of the $MAPbI_3$/G-NH_2-based PSC revealed by impedance spectroscopy (EIS) characteristics under illumination in Fig. S14 (ESI†) also confirms the better charge transfer compared to the $MAPbI_3$-based PSC (~33 Ω). In addition, the significant enhancement of FF in the former case could be due to the efficient charge extraction and transport by the nano-network

 This journal is © The Royal Society of Chemistry 2018

Published on 21 June 2018. Downloaded by Brown University on 4/15/2019 6:26:14 PM.

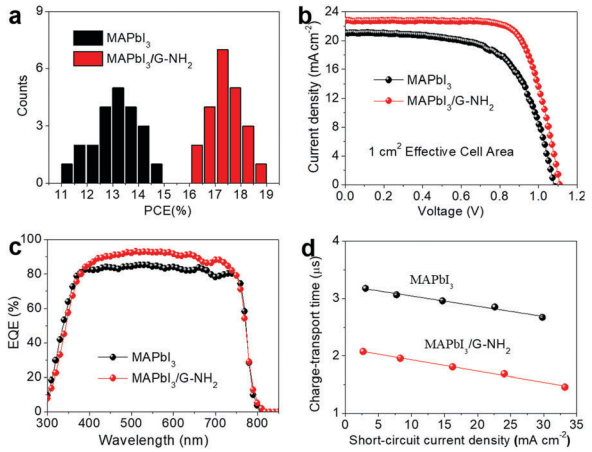

Fig. 2 (a) PCE distributions of PSCs based on $MAPbI_3$ with and without G-NH_2 (average of 22 devices), (b) J–V characteristics for PSCs of 1×1 cm^2 based on $MAPbI_3$ with and without G-NH_2 under simulated AM 1.5G solar illumination of 100 mW cm^{-2} in reverse scan, and (c) corresponding EQE spectrum together with the integrated J_{SC}. (d) Charge transport time dependence on the J_{SC} of PSCs based on $MAPbI_3$ with and without G-NH_2 measured using the IMPS technique.

as PSC FF is closely related to additional charge transport losses originating from inefficient charge extraction of the cells, or current leakage through shunts.[36]

A previous report has revealed that the lower charge extraction and transport limited the photocurrent observed in the $MAPbI_3$ PSCs.[37] Intensity modulated photocurrent spectroscopy (IMPS) measurements were performed on the $MAPbI_3$- and $MAPbI_3$/G-NH_2-based PSCs to explore the impact of the nano-network on the charge-transport properties. The charge transport in the $MAPbI_3$/G-NH_2-based PSC is faster than that in the $MAPbI_3$-based PSC (Fig. 2d). This confirms that the incorporation of the G-NH_2 nano-network in the perovskite absorber layer facilitates charge extraction and transport for a higher charge-collection efficiency. Other than the higher charge-collection efficiency and higher performance, the $MAPbI_3$/G-NH_2-based PSCs exhibit better stability than PSCs based on pure $MAPbI_3$ perovskite in a dark box with 20–30% relative humidity (RH) and at a temperature of 25–30 °C. The $MAPbI_3$/G-NH_2-based PSC without any encapsulation still maintains ~17% PCE after 2 months of storage, whereas the PCE of the $MAPbI_3$-based device drops to ~8% (Fig. S15, ESI†).

Conducting atomic force microscopy (c-AFM) in contact mode was performed to investigate the effect of the nano-networks on charge transport. Fig. 3 shows that the average currents through $MAPbI_3$ and $MAPbI_3$/G-NH_2 thin films are 198 pA and 301 pA, respectively, under 1 V direct-current (DC) bias. The current in the $MAPbI_3$/G-NH_2 thin film is more unevenly distributed over the surface in comparison with the pure $MAPbI_3$ thin film. Interestingly, the current is most prominent in the GB region (G-NH_2) in the $MAPbI_3$/G-NH_2 thin film as shown in Fig. 3e and f. These results indicate that the G-NH_2 present at the GBs exhibits excellent charge transport capability.

The aforementioned results suggest that the observed improvement in the J_{SC} and FF of $MAPbI_3$/G-NH_2-based PSCs could be attributed to the efficient charge collection by the G-NH_2-based nano-networks incorporated within the perovskite absorber layer. Usually, the defects/traps in the perovskite layer can result in recombination of charge carriers (the left image in Fig. 4a), and cause a decrease in J_{SC}, V_{OC}, and, especially, FF, causing further reduction in the PCE. In fact, the defects/traps induce even more serious issues in large-area PSCs.[38,39] In our study, the plausible working mechanism behind this high current collection efficiency could be attributed to bypassing defect sites *via* the nano-network as shown in the right image in Fig. 4a.

We further calculate the charge density at the interface of $MAPbI_3$ with G-NH_2, using the density-functional theory (DFT) method, as shown in Fig. 4b. It can be seen that there is a significant charge rearrangement at the interface of G-NH_2 with $MAPbI_3$, forming an internal electrical field near the interface. Specifically, the negative charges gather near the G-NH_2 while the positive charges gather near the surface in $MAPbI_3$ perovskite,

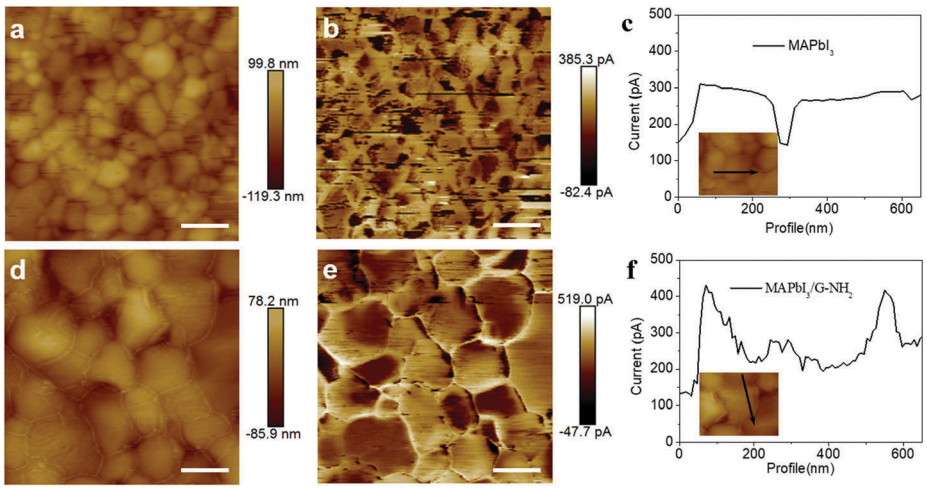

Fig. 3 $MAPbI_3$ thin film: (a) topographic image film and (b) corresponding current image (1 V applied DC voltage), (c) c-AFM current line profiles for $MAPbI_3$. Inset: Corresponding topographic AFM images. $MAPbI_3$/G-NH_2 thin film: (d) topographic image and (e) corresponding current image (1 V applied DC voltage), (f) c-AFM current line profiles for the $MAPbI_3$/G-NH_2 thin film. Inset: Corresponding topographic AFM images. Scale bars = 400 nm.

Published on 21 June 2018. Downloaded by Brown University on 4/15/2019 6:26:14 PM.

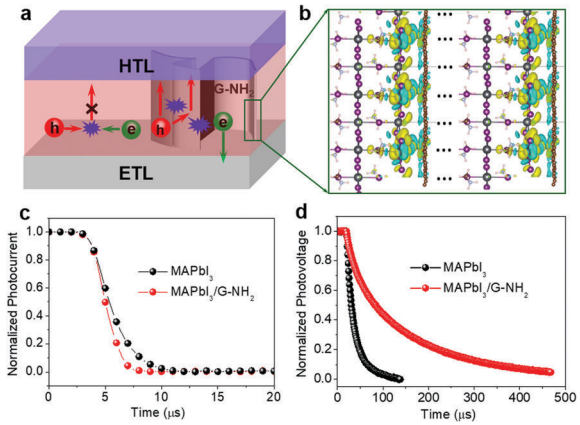

Fig. 4 (a) Schematic illustrations of charge transport in a PSC based on $MAPbI_3$ without and with G-NH_2. (b) Calculated charge density at the interface between $MAPbI_3$ and G-NH_2 (yellow = positive, cyan = negative). Large-area (1 cm^2) PSCs based on $MAPbI_3$ with and without G-NH_2: (c) TPC and (d) TPV.

resulting in dipoles pointing from $MAPbI_3$ to G-NH_2. This newly produced dipole field facilitates the hole transfer into G-NH_2 from $MAPbI_3$ perovskite. For comparison, we also present the charge density at the interface of $MAPbI_3$ perovskite and rGO without a functionalized amino group in Fig. S16 (ESI†), where it shows a much weaker internal electrical field at the interface. This theoretical result supports the notion that the nano-network based on G-NH_2 can significantly promote charge transfer, and it also confirms that the chemisorbed amino functional group is likely responsible for these observed enhancements.

The incorporation of rGO into the $MAPbI_3$ perovskite absorber layer does not lead to significant improvements in PV performance (Fig. S17, ESI†). Furthermore, the longer PL lifetime indicates that the rGO may work mainly as a passivation layer in the $MAPbI_3$/rGO thin film.[30,40] These experimental results on rGO are consistent with the theoretical calculations (Fig. S16, ESI†).

The charge transport in the large-area devices was further investigated by transient photocurrent decay and photovoltage decay (TPC/TPV). The faster photocurrent decay response of the $MAPbI_3$/G-NH_2-based PSC illustrates faster charge transport than in the $MAPbI_3$-based PSC (Fig. 4c). Meanwhile, the TPV decay curve of the $MAPbI_3$/G-NH_2-based PSC shows a longer lifetime than that of the $MAPbI_3$-based PSC, indicating a significant decrease in charge-carrier recombination (Fig. 4d). We attribute the reduced recombination to the improvement of extraction and transport of charge carriers by the G-NH_2 nano-network. The improvements in the extraction and transport of charge-carriers in the perovskite layer is beneficial for improving the J_{SC}, V_{OC}, and, especially, FF.

Conclusions

In summary, we have successfully demonstrated the construction of a charge-collection nano-network in PSCs by incorporating graphene with functionalized amino groups into the $MAPbI_3$ perovskite absorber layer. This nano-network induces dramatically higher charge-extraction efficiency, facilitates charge transport, and finally leads to significantly enhanced PCE of large area PSCs. Planar large-area (1 cm^2) PSCs incorporating this nano-network have PCEs close to 19%, with excellent reproducibility. The approach and strategy of incorporating the charge-collection nano-network could be applied to other perovskite compositions, and even to other types of solar cells, and it represents a promising new concept for achieving high-performance PVs in the future.

Author contributions

Y. Zhao conceived the idea, directed and supervised the project. Y. W. fabricated devices. Y. W, Y. Zhou. T. Z., M. J., L. Z., M. K., Y. L., X. Z. were involved in experimental and theoretical data analysis. All authors contributed to the discussions. Y. Zhao, Y. W., Y. Zhou, and N. P. P co-wrote the manuscript.

Conflicts of interest

There are no conflicts to declare.

Acknowledgements

Y. Zhao acknowledges the support of the NSFC (Grant 21777096) and Huoyingdong Grant (151046). The work performed at Brown University and UNL was supported by the U.S. National Science Foundation (No. OIA-1538893).

References

1 H. Chen, F. Ye, W. Tang, J. He, M. Yin, Y. Wang, F. Xie, E. Bi, X. Yang, M. Gratzel and L. Han, *Nature*, 2017, **550**, 92–95.
2 Z. Xiao, Y. Yuan, Q. Wang, Y. Shao, Y. Bai, Y. Deng, Q. Dong, M. Hu, C. Bi and J. Huang, *Mater. Sci. Eng., R*, 2016, **101**, 1–38.
3 A. Mei, X. Li, L. Liu, Z. Ku, T. Liu, Y. Rong, M. Xu, M. Hu, J. Chen, Y. Yang, M. Grätzel and H. Han, *Science*, 2014, **345**, 295–298.
4 NREL, https://www.nrel.gov/pv/assets/images/efficiency-chart.png.
5 N. J. Jeon, J. H. Noh, Y. C. Kim, W. S. Yang, S. Ryu and S. I. Seok, *Nat. Mater.*, 2014, **13**, 897–903.
6 Y. Zhao and K. Zhu, *J. Phys. Chem. Lett.*, 2014, **5**, 4175–4186.
7 N. G. Park, M. Grätzel, T. Miyasaka, K. Zhu and K. Emery, *Nat. Energy*, 2016, **1**, 16152.
8 D. W. Dequilettes, S. M. Vorpahl, S. D. Stranks, H. Nagaoka, G. E. Eperon, M. E. Ziffer, H. J. Snaith and D. S. Ginger, *Science*, 2015, **348**, 683–686.
9 D. Y. Son, J. W. Lee, Y. J. Choi, I. H. Jang, S. Lee, P. J. Yoo, H. Shin, N. Ahn, M. Choi, D. Kim and N. G. Park, *Nat. Energy*, 2016, **1**, 16081.
10 L. Meng, J. You, T. F. Guo and Y. Yang, *Acc. Chem. Res.*, 2016, **49**, 155–165.
11 M. Liu, M. B. Johnston and H. J. Snaith, *Nature*, 2013, **501**, 395–398.

 This journal is © The Royal Society of Chemistry 2018

Published on 21 June 2018. Downloaded by Brown University on 4/15/2019 6:26:14 PM.

12 F. Wang, W. Geng, Y. Zhou, H. H. Fang, C. J. Tong, M. A. Loi, L. M. Liu and N. Zhao, *Adv. Mater.*, 2016, **28**, 9986–9992.
13 H. Tan, A. Jain, O. Voznyy, X. Lan, F. P. G. de Arquer, J. Z. Fan, R. Quintero-Bermudez, M. Yuan, B. Zhang, Y. Zhao, F. Fan, P. Li, L. N. Quan, Y. Zhao, Z.-H. Lu, Z. Yang, S. Hoogland and E. H. Sargent, *Science*, 2017, **355**, 722–726.
14 S. D. Stranks, G. E. Eperon, G. Grancini, C. Menelaou, M. J. Alcocer, T. Leijtens, L. M. Herz, A. Petrozza and H. J. Snaith, *Science*, 2013, **342**, 341–344.
15 G. Xing, N. Mathews, S. Sun, S. S. Lim, Y. M. Lam, M. Grätzel, S. Mhaisalkar and T. C. Sum, *Science*, 2013, **342**, 344–347.
16 C. H. Chiang and C. G. Wu, *Nat. Photonics*, 2016, **10**, 196–200.
17 L. Zuo, H. Guo, D. W. Dequilettes, S. Jariwala, N. D. Marco, S. Dong, R. Deblock, D. S. Ginger, B. Dunn, M. Wang and Y. Yang, *Sci. Adv.*, 2017, **3**, e1700106.
18 J. Xu, A. Buin, A. H. Ip, W. Li, O. Voznyy, R. Comin, M. Yuan, S. Jeon, Z. Ning, J. J. McDowell, P. Kanjanaboos, J. P. Sun, X. Lan, L. N. Quan, D. H. Kim, I. G. Hill, P. Maksymovych and E. H. Sargent, *Nat. Commun.*, 2015, **6**, 7081.
19 I. J. Park, G. Kang, M. A. Park, J. S. Kim, S. W. Seo, D. H. Kim, K. Zhu, T. Park and J. Y. Kim, *ChemSusChem*, 2017, **10**, 2660–2667.
20 M. Yang, Y. Zhou, Y. Zeng, C. S. Jiang, N. P. Padture and K. Zhu, *Adv. Mater.*, 2015, **27**, 6363–6370.
21 X. Fang, J. Ding, N. Yuan, P. Sun, M. Lv, G. Ding and C. Zhu, *Phys. Chem. Chem. Phys.*, 2017, **19**, 6057–6063.
22 C. Park, H. Ko, D. H. Sin, K. C. Song and K. Cho, *Adv. Funct. Mater.*, 2017, **27**, 1703546.
23 J. T. Wang, J. M. Ball, E. M. Barea, A. Abate, J. A. Alexander-Webber, J. Huang, M. Saliba, I. Mora-Sero, J. Bisquert, H. J. Snaith and R. J. Nicholas, *Nano Lett.*, 2014, **14**, 724–730.
24 P. You, Z. Liu, Q. Tai, S. Liu and F. Yan, *Adv. Mater.*, 2015, **27**, 3632–3638.
25 Z. Liu, P. You, C. Xie, G. Tang and F. Yan, *Nano Energy*, 2016, **28**, 151–157.
26 J. H. Im, I. H. Jang, N. Pellet, M. Gratzel and N. G. Park, *Nat. Nanotechnol.*, 2014, **9**, 927–932.
27 Y. Rong, Z. Tang, Y. Zhao, X. Zhong, S. Venkatesan, H. Graham, M. Patton, Y. Jing, A. M. Guloy and Y. Yao, *Nanoscale*, 2015, **7**, 10595–10599.
28 Y. Zhou, O. S. Game, S. Pang and N. P. Padture, *J. Phys. Chem. Lett.*, 2015, **6**, 4827–4839.
29 F. Ji, S. Pang, L. Zhang, Y. Zong, G. Cui, N. P. Padture and Y. Zhou, *ACS Energy Lett.*, 2017, **2**, 2727–2733.
30 M. Hadadian, J. P. Correa-Baena, E. K. Goharshadi, A. Ummadisingu, J. Y. Seo, J. Luo, S. Gholipour, S. M. Zakeeruddin, M. Saliba, A. Abate, M. Gratzel and A. Hagfeldt, *Adv. Mater.*, 2016, **28**, 8681–8686.
31 N. Arora, M. I. Dar, A. Hinderhofer, N. Pellet, F. Schreiber, S. M. Zakeeruddin and M. Grätzel, *Science*, 2017, **358**, 768.
32 S. Song, G. Kang, L. Pyeon, C. Lim, G.-Y. Lee, T. Park and J. Choi, *ACS Energy Lett.*, 2017, **2**, 2667–2673.
33 W. Chen, F.-Z. Liu, X.-Y. Feng, A. B. Djurišić, W. K. Chan and Z.-B. He, *Adv. Energy Mater.*, 2017, **7**, 1700722.
34 Y. Zhou, A. L. Vasiliev, W. Wu, M. Yang, S. Pang, K. Zhu and N. P. Padture, *J. Phys. Chem. Lett.*, 2015, **6**, 2292–2297.
35 H.-C. Liao, P. Guo, C.-P. Hsu, M. Lin, B. Wang, L. Zeng, W. Huang, C. M. M. Soe, W.-F. Su, M. J. Bedzyk, M. R. Wasielewski, A. Facchetti, R. P. H. Chang, M. G. Kanatzidis and T. J. Marks, *Adv. Energy Mater.*, 2017, **7**, 1601660.
36 M. Stolterfoht, C. M. Wolff, Y. Amir, A. Paulke, L. PerdigónToro, P. Caprioglio and D. Neher, *Energy Environ. Sci.*, 2017, **10**, 1530–1539.
37 A. Pockett, G. E. Eperon, T. Peltola, H. J. Snaith, A. Walker, L. M. Peter and P. J. Cameron, *J. Phys. Chem. C*, 2015, **119**, 3456–3465.
38 R. Long, J. Liu and O. V. Prezhdo, *J. Am. Chem. Soc.*, 2016, **138**, 3884–3890.
39 D. Zhao, M. Sexton, H. Y. Park, G. Baure, J. C. Nino and F. So, *Adv. Energy Mater.*, 2015, **5**, 1401855.
40 J. S. Yeo, R. Kang, S. Lee, Y. J. Jeon, N. Myoung, C. L. Lee, D. Y. Kim, J. M. Yun, Y. H. Seo, S. S. Kim and S. I. Na, *Nano Energy*, 2015, **12**, 96–104.